Seedless Growth of Sub-10 nm Germanium Nanowires

Richard G. Hobbs[†,ϕ], Sven Barth[†,ϕ], Nikolay Petkov[‡], Michaela Zirngast[#], Christoph Marschner[#],

Michael A. Morris and Justin D. Holmes[,†,ϕ]*

Materials and Supercritical Fluids Group, Department of Chemistry and the Tyndall National Institute, University College Cork, Cork, Ireland. Centre for Research on Adaptive Nanostructures and Nanodevices (CRANN), Trinity College Dublin, Dublin 2, Ireland. Electron Microscopy and Analysis Facility (EMAF), Tyndall National Institute, Lee Maltings, Prospect Row, Ireland. Institut für Anorganische Chemie der Technischen Universität Graz, Stremayrgasse 16, A-8010 Graz, Austria.

[*]Corresponding author, j.holmes@ucc.ie, tel. +353 21 4903608, fax +353 21 4274097

RECEIVED DATE (to be automatically inserted after your manuscript is accepted if required according to the journal that you are submitting your paper to)

[†]Materials and Supercritical Fluids Group, Department of Chemistry and the Tyndall National Institute, University College Cork, Ireland.

[ϕ]Centre for Research on Adaptive Nanostructures and Nanodevices (CRANN), Trinity College Dublin, Dublin 2, Ireland

[‡]Electron Microscopy and analysis Facility, Tyndall National Institute, Cork, Ireland

#Institut für Anorganische Chemie der Technischen Universität Graz, Austria.

Abstract

We report the self-seeded growth of highly crystalline Ge nanowires, with a mean diameter as small as 6 nm without the need for a metal catalyst. The nanowires, synthesized using the purpose-built precursor hexakis(trimethylsilyl)digermane, exhibit high aspect ratios (> 1000) whilst maintaining a uniform core diameter along their length. Additionally, the nanowires are encased in an amorphous shell of material derived from the precursor, which acts to passivate their surfaces and isolate the Ge seed particles from which the nanowires grow. The diameter of the nanowires was found to depend on the synthesis temperature employed. Specifically, there is a linear relationship between the inverse radius of the nanowires and the synthesis temperature, which can be explained by a model for the size-dependent melting of simple metals.

Introduction

The bottom-up assembly of semiconductor nanowires could potentially lead to the future miniaturization of microelectronic devices.[1, 2] Semiconductors which are compatible with current Si processing techniques are of particular interest, in order to minimize the cost and number of processing steps required for their integration into current manufacturing procedures. Si and Ge are examples of two such semiconductors, where Ge offers a number of distinct advantages over Si. For instance, charge carriers in Ge have lower effective masses than in Si resulting in two important connotations. Firstly, the effective mass of the charge carrier is inversely related to carrier mobility, giving charge carriers in Ge increased mobility relative to Si.[3] Likewise, the exciton Bohr radius is inversely proportional to the effective mass of the charge carrier pair (exciton), implying that Ge will begin to exhibit potentially exploitable quantum confinement properties at larger dimensions (24.3 nm) compared to Si (4.9 nm). However, significant quantum confinement effects will not be observed until dimensions well below these exciton Bohr radii values are achieved. For example, Ge nanowires do not display noticeable quantum confinement effects at diameters above 10 nm.[4]

Gold or similar catalytic colloidal metal particles are generally used to seed the growth of semiconductor nanowires, in accordance with the vapor-liquid-solid (VLS) growth mechanism proposed by Wagner and Ellis.[5] A high solubility of the semiconductor material in the catalytic metal seed is crucial to enable the VLS pathway to crystalline nanowire formation. However, the high solubility of the semiconductor material in the metal seed means that metal atoms are inevitably drawn into the crystalline nanowire matrix, resulting in detrimental effects on the electrical properties of the nanowires.[6] Perea *et al.*[7] have recently made attempts to detect and measure the concentration of dopant metal atoms in semiconductor nanowires introduced by the VLS method.[8]

This work demonstrates for the first time, that high aspect ratio Ge nanowires with mean diameters below 10 nm and lengths up to 20 μm, can be synthesized by bottom-up techniques in the absence of a metal catalyst seed. Instead the nanowires grow directly from liquid Ge droplets within a silicon-based matrix. Few reports of Ge nanowires produced in the absence of a foreign catalytic seed particle exist and none of these studies have produced long, straight, Ge nanowires with mean diameters below 10 nm and a low defect density. Ge *et al.*[9] reported the synthesis of Ge nanowires by the decomposition of the Ge salt $[(CH_3(CH_2)_7CHCH(CH_2)_7CH_2NH_2)_4Ge]^{4+}(Cl^-)_4$, in trioctylamine at 360 °C. They found a correlation between the amount of precursor used in the reaction and the mean diameter of the nanowires obtained (≥ 15 nm as determined using the Scherrer expression), and suggested a VLS-type growth mechanism from liquid Ge droplets.[10] Zaitseva *et al.*[11] reported the synthesis of Ge nanowires from tetraethylgermane, and attributed nanowire growth to a VLS mechanism whereby the liquid seed took the form of nanoscale droplets of high boiling point hydrocarbon material produced from the polymerization of the ethyl radicals liberated during the precursor decomposition process. These nanowires exhibited a broad range of diameters, spanning from 5 to 700 nm. Zhang *et al.*[12] have applied an oxide assisted growth (OAG) technique to synthesize Ge nanowires. The technique, which involves laser ablating Ge in the presence of GeO_2 has been used to produce Ge-GeO_2 core-shell nanowires with core diameters ranging from 6 to 17 nm, and which possess an undulating core-shell

interface. Meng *et al.*[13] have also produced Ge-SiO_x core-shell nanowires with crystalline Ge nanowire core diameters between 30-100 nm. These nanowires were grown by thermal evaporation of SiO and Ge powders, and a combined OAG/VLS growth mechanism was suggested. Ge/SiC_xN_y core/shell nanocables have been synthesized by Mathur *et al.*[14] from $Ge(N(SiMe_3)_2)_2$ using a chemical vapor deposition (CVD) approach. They assumed a self-seeded VLS-type growth mechanism for these nanocables, which had a core diameter of ~ 60 nm. Lastly, Gerung *et al.*[15] have produced kinked Ge nanowires using a Ge^{2+} alkoxide precursor. They suggested two possible growth mechanisms; VLS growth from Ge nanoparticles and self assembly via homogeneous nucleation. The lowest mean nanowire diameter achieved using this approach was 6 nm, with a mean nanowire length of 50 nm. These reports, apart from the OAG method, suggest a VLS growth mechanism for the formation of Ge nanowires. Furthermore, only the work of Gerung *et al.* reports a mean Ge nanowire diameter as low as that reported here. However, these nanowires had low aspect ratios (< 10) and the crystals produced contained many defects.

As stated earlier, a liquid seed droplet is a prerequisite for the VLS growth of Ge nanowires. The aim of this work was therefore, not only to demonstrate the synthesis of Ge nanowires in the absence of a foreign metal seed catalyst, but also to exploit the exaggerated melting point depression of Ge at the nanoscale in order to control the diameter of the nanowires produced. The choice and design of a suitable precursor is key, in order to prevent aggregation and coarsening of Ge nanocrystals resulting in undesirable microparticles. In addition, the selection of an appropriate synthesis temperature is essential to optimize the quality and quantity of the nanowires produced. The temperature chosen must be sufficiently high to allow precursor decomposition, and liberation of Ge atoms, but also be low enough to prevent coagulation of Ge nuclei forming particles of larger diameters. To date, nanowire diameter control has been achieved either through the use of pre-synthesized colloidal seed metal particles[16], or porous substrates which act as templates or moulds for the nanowires.[17, 18] This work demonstrates that a pre-synthesized metal seed particle is not required to exert control over the diameter of Ge nanowires.

Exploitation of the melting point depression of materials at the nanoscale to control the dimensions of nanowires has previously been suggested.[19, 20] However, these suggestions were again made for metal-catalyzed nanowire growth and specifically the use of the depressed Au-Ge eutectic point at the nanoscale to control nanowire diameters.

The nanowires reported here were produced in solution and within a supercritical fluid (SCF) medium using the metalorganic precursors hexakis(trimethylsilyl)digermane ($Ge_2(TMS)_6$) and tris(trimethylsilyl)germane ($HGe(TMS)_3$). The nanowires were sheathed in a layer of amorphous material, composed of Si, C, O and Ge. This shell is representative of the decomposed precursor material that did not form Ge nanowires, and acted to passivate the nanowires. This work follows on from the previous report made by our group on the growth of Ge/SiO_x, core/shell nanocables, from $Ge_2(TMS)_6$ via gold and nickel-catalyzed VLS growth.[21] The gold and nickel catalyzed nanowires were found to grow faster and with larger diameters than those grown from $Ge_2(TMS)_6$ in the absence of such metal seeds.

Experimental

Hexakis(trimethylsilyl)digermane was synthesized as described in the literature.[22] High temperature synthesis (> 703 K) of Ge nanowires was performed in a supercritical toluene medium using a setup similar to that described previously.[23] In a typical experiment 100 mg of $Ge_2(TMS)_6$ was dissolved in 10 mL of dry, oxygen-free toluene and loaded into a 20 mL stainless steel precursor reservoir. Separately, 1 mL of toluene was loaded into a 5 mL volume, stainless steel reaction cell, which was connected to the precursor reservoir by 1/16" stainless steel tubing and valves. Precursor dissolution and loading was performed within a nitrogen filled glove-box (O_2 < 0.2 ppm, H_2O < 3 ppm) to help prevent the formation of GeO_2. The sealed reaction cell was then placed in a tube furnace and heated to the desired synthesis temperature, which was monitored by a thermocouple connected to the reaction vessel. Whilst the reaction cell was heating, 17.2 MPa pressure was applied to the precursor solution in

the reservoir and injected at the chosen synthesis temperature using a CO_2 pump (ISCO systems). The volume of the precursor solution injected into the cell was dependent on the pressure difference between the reaction cell and the pressure applied to the precursor reservoir by the CO_2 pump. This pressure difference could be controlled by the volume of toluene placed in the reaction cell prior to heating. Typically, 2.5±0.3 mL of precursor solution was injected into the reaction cell and the holding time was adjusted according to the temperature employed for a high yield of Ge nanowires. Synthesis times required to produce Ge nanowires for each synthesis temperature are tabulated in the Supporting Information (table S1). The cell was opened at room temperature, the initial solvent collected and combined with an acetone solution used to collect the nanowire material attached to the side walls of the reactor. The red/brown nanowire product was isolated from the solvents by evaporation. Further purification of the nanowire material was performed by centrifugation at room temperature (7000 rpm for 15 mins; 3× toluene, and 2× ethanol).

In a separate approach, in order to confirm that the wires were not seeded from Fe or Ni in the walls of the stainless steel cell, Ge nanowires exhibiting the same morphology as those synthesized by the method described above were prepared under atmospheric pressure using standard Schlenk line techniques, similar to the procedure described by Heitsch *et al.*[24] for the preparation of Si nanowires from Au and Bi nanoparticles. 100 mg of $Ge_2(TMS)_6$ was placed in a 3-necked 50 mL round bottomed flask with 5 g of dried octacosane (b.p. 703 K) and connected to the Schlenk line. Argon gas was passed through the flask and the temperature of the solution was raised to 673 K for 24 h to enable the decomposition of the Ge precursor, and the growth of nanowires. During the cooling step 20 mL of hexane was injected at 343 K into the flask. The hexane helps to dissolve the octacosane (m.p. 330-335 K) which begins to solidify below 333 K. The nanowire product was further purified by centrifugation (7000 rpm for 20 min; 2× toluene and 2× ethanol) to ensure maximum removal of octacosane.

X-ray diffraction data were collected on a Phillips Xpert PW3719 diffractometer using Cu K_α radiation (40 kV and 35 mA) over the range $20 \leq 2\theta \leq 70$. A JEOL 2000FX transmission electron microscope (TEM) operating at an acceleration voltage of 200 kV was used for TEM bright field imaging as well as selective area electron diffraction (SAED). Energy dispersive x-ray (EDX) analysis was performed using an Oxford Instruments INCA energy system fitted to the TEM. High resolution TEM (HRTEM) images and high-angle annular dark-field (HAADF) scanning TEM images were collected using a JEOL 2010F HRTEM instrument operating at an acceleration voltage of 200 kV. In all cases, samples were prepared for analysis by sonicating the material in acetone before TEM sample preparation.

Results and Discussion

The series of experiments performed in this work revealed a relationship between the chosen synthesis temperature and the diameter distribution of the Ge nanowires produced from $Ge_2(TMS)_6$. This relationship is highlighted in figures 1 and 2. Figure 1 shows a plot of the percentage of nanowires obtained with a given diameter for each of the four synthesis temperatures employed. Each trace in this plot represents a Lorentzian fit to the raw data which was obtained by direct measurement of the nanowire diameters using TEM. The raw data is included in the Supporting Information (figure S1) as are a selection of TEM micrographs of Ge nanowires grown at each of the synthesis temperatures employed in this work (figures S2-S5). A distinct increase in the centre of the Lorentzian distribution was observed as the synthesis temperature increased. The observed relationship between temperature and nanowire radius is indicative of a thermally controlled nanowire growth process.

Since its conception in 1910 the Lindeman criterion has been shown to accurately describe the melting of simple metals, *i.e.* close-packed arrangements of atoms.[25] Central to the Lindemann criterion is the relationship between the root-mean-square thermal average amplitude of vibration of an atom in a crystal, and temperature. The criterion states that when the amplitude of vibration of an atom in a

material reaches a threshold value, melting ensues. This threshold value is approximately equal to 10 % of the mean interatomic separation in that material. Melting is known in many cases to initiate at the surface of materials where separation of atoms differs significantly from that within the bulk.[26] Nanoscale materials such as nanowires and nanoparticles exhibit a high surface to volume ratio, and as such can be expected to melt at lower temperatures than their bulk counterparts. Recently, a model has been derived to describe the relationship between the melting temperature and particle size based on the Lindeman criterion,[27] $T_r/T_o = \exp[-2(S_m - R)/(3R(r/r_o - 1))]$, where T_r and T_o are the melting points of the nanocrystal and the bulk material respectively, r_o represents the critical radius at which all of the atoms of the nanocrystal are at the surface, r denotes the particle/wire radius, R is the ideal gas constant, and S_m is the bulk melting entropy (31.1 $JK^{-1}mol^{-1}$ for Ge).[28] The critical radius r_o can be determined from the expression, $r_o = (3 - d)(6\Omega/\pi)^{1/3}$, where d denotes the dimension of the solid (d = 0 for nanoparticles, d = 1 for nanowires and d = 2 for thin films), and Ω denotes the volume per atom in the bulk solid material. The choice of an appropriate value of r_o for the nanowires produced in this work requires a number of considerations. If we assume a supercritical fluid-liquid-solid (SFLS) or solution-liquid-solid (SLS) growth mechanism for the nanowires, the Ge nanoparticles should preferentially exist in a liquid state at the synthesis temperature to act as seeds for the SFLS/SLS growth of Ge nanowires. Furthermore, the nanowires produced must be sufficiently large in diameter to exist as a solid at the synthesis temperature. It is well known that the interface between a solid wire and a liquid particle is important in the VLS growth of nanowires, and ultimately that it can determine the diameter of the nanowires formed.[29] Given that during the VLS growth of a Ge nanowire from a Ge seed, where the seed particle is in the liquid state and the nanowire is in the solid state, the interface of the wire and seed must be exactly at the melting point, *i.e.* at the phase boundary between liquid Ge and solid Ge. Therefore, the value of r_o chosen must lie between that of a nanowire (r_o = 0.702 nm) and that of a nanoparticle (r_o = 1.053 nm). The value of r_o used here was 0.88 nm, midway between that of a nanoparticle a nanowire. The solid trace in figure 2 represents a plot of T_r against 1/r using the model outlined above. The model is pseudo-linear for the range of values of 1/r shown in figure 2. The plot

intercepts the y-axis at 1211 K, the bulk melting temperature of Ge. The dashed trace represents a linear fit to the four mean radii obtained from the plots in figure 1, and clearly correlates well with the model described herein.

A distinct increase in the diameter distribution with increasing temperature is also apparent from the data shown in figure 1. The full-width at half maximum (FWHM) of the Lorentzian distribution of diameters for nanowires synthesized at 573 K was 2.0 nm, compared to a FWHM value of 3.0 nm for nanowires produced at 773 K. The broader distribution at 773 K may be attributed to two factors. Smaller diameter wires may form at temperatures below 773 K as the room temperature precursor solution is injected into the reactor. Also, larger diameter wires may form by a solid-phase seeding mechanism as larger Ge particles would exist in the solid phase at 773 K.

Figure 3(a) shows a TEM micrograph of a typical Ge nanowire grown at 773 K from $Ge_2(TMS)_6$ using the high pressure method outlined above. This micrograph clearly shows the core-shell morphology of the nanowires produced at these temperatures, as observed by the contrast difference between the dark Ge core, and the lighter amorphous shell. The nanowire has a 10 nm diameter, crystalline Ge core. Figure 3(c) (inset) shows a higher magnification HRTEM micrograph of a similar 10 nm diameter nanowire with a 3 nm thick shell. This HRTEM micrograph was recorded along the <111> zone axis of the crystalline nanowire. Figure 3(b) displays a FFT image of figure 3(c) and highlights the low defect density present in the Ge nanowire core. A <211> crystal growth direction can be inferred from the FFT of the HRTEM micrograph. The Ge nanowires produced in this work generally exhibit <110> growth directions, whilst approximately 25 % of the nanowires analysed were oriented along the <211> crystal axes. No <111> oriented nanowires were observed amongst the nanowires produced in this work. This observation is consistent with reports on the diameter dependent growth direction of Si nanowires produced by CVD using Au catalyst. Schmidt *et al*.[30] found that growth of <110> oriented Si nanowires is more prevalent than growth of <211> or <111> oriented nanowires, for nanowires less

than 20 nm in diameter. Given that Si and Ge share the same crystal symmetry, a similar size-dependent nanowire growth direction may be expected for Ge.

Figure 4 displays a SEM micrograph highlighting the high density of nanowires produced using the methods outlined above. The SEM micrograph also emphasizes the high aspect ratio of the nanowires produced. Inset in figure 4 is a HAADF STEM micrograph of three Ge nanowires produced at 673 K. The distinct contrast difference between the Ge nanowire core and the amorphous Si-based shell emphasizes the core-shell morphology of the nanowires. The image also highlights the uniformity of the core diameter relative to the shell thickness. Hence, whilst the amorphous shell is non-uniform in thickness the core diameter remains uniform along the length of the nanowires.

An XRD pattern of a sample of these nanowires is shown in figure 5. The most intense reflections can be indexed to cubic Ge (JCPDS, reference pattern 04-0545, space group *Fd3m*). The broad reflections are characteristic of the nanoscale dimensions of small diameter nanowires and minor Ge nanoparticle by-products. The broad hump in the baseline of the XRD pattern between 40 and 60 °2θ could be attributed to the amorphous Si-based matrix present in the nanowire sample. This Si-based by-product has been investigated by EDX and TEM, and was found to be composed of Ge, Si, C, & O. SAED of some of the smaller particulate by-product revealed that the material was largely amorphous in nature although it did have some polycrystalline component. The polycrystalline component could be attributed to Ge nanoparticles present within an amorphous matrix.

The shell of the amorphous material found on Ge nanowires produced at higher temperatures was investigated by EDX analysis. Three 8 nm diameter nanowires with different shell thicknesses (5 nm, 10 nm, and 20 nm) were examined. EDX revealed Si/Ge atomic ratios of 4.0, 4.5 and 5.5 for the wires with 5 nm, 10 nm and 20 nm shells respectively. This investigation suggests that the amorphous shell is largely composed of Si. However, the Si/Ge ratio would be expected to increase more significantly if

the shell was purely amorphous Si or SiO_2, suggesting that Ge or C are also present. Furthermore, FTIR analysis of a sample of nanowires produced at 723 K (see Supporting Information, figure S6) revealed strong Si-O vibrational modes at 460 cm^{-1}, and 1080 cm^{-1}. Weaker Si-O vibrational modes were also observed at 565 cm^{-1}, 798 cm^{-1}, and 1153 cm^{-1}. The broad peak at approximately 1225 cm^{-1} could be attributed to a Si-O-C vibrational mode. The weak peak at 1489 cm^{-1} may be attributed to a $Si-CH_2$ scissor mode and the other weak peaks at 2855 cm^{-1} and 2927 cm^{-1} can be assigned to the vibrational modes of alkyl groups.[31, 32] The FTIR data tentatively suggests that the trimethylsilyl (TMS) groups in the precursor are partially decomposed during the synthesis process. The weak $Si-CH_2$ and alkyl vibrational modes suggest that some of the TMS groups remain intact following nanowire synthesis, but, the intense Si-O vibrational modes suggest that many of the TMS groups decompose to produce Si which is subsequently partially oxidized by reaction with trace levels of water present in the system. The composition of the shell material coating the Ge nanowires cannot be stated conclusively as the FTIR spectrum was recorded for all the material present in the sample which includes Ge nanowires coated in an amorphous shell, as well as the particulate by-product.

Experiments using $HGe(TMS)_3$ as a precursor to generate Ge nanowires were found to require longer synthesis times than those required for $Ge_2(TMS)_6$ to produce an identical nanowire product, although in lower yield. The longer synthesis time, approximately double that required for $Ge_2(TMS)_6$ to produce nanowires, may be attributed to the slower decomposition kinetics of the precursor. However, it is also possible that the evolution of hydrogen upon cleavage of the Ge-H bond in $HGe(TMS)_3$ has an adverse effect on the nanowire growth process. A TEM micrograph of a typical nanowire produced at 673 K from this precursor can be seen in the Supporting Information (figure S7). The nanowire closely resembles those produced from $Ge_2(TMS)_6$. A Lorentzian fit (R^2 = 0.73, FWHM = 3.0 nm) to a plot of percentage nanowires against Ge nanowire diameter, for these nanowires was centered at a diameter of 7.1 nm. This is in good agreement with the value of 7.1 nm obtained for Ge nanowires produced from $Ge_2(TMS)_6$ at 673 K.

In an attempt to clarify the growth mechanism of the Ge nanowires a number of other experiments were performed. Firstly, experiments using synthesis temperatures below 703 K were performed in glassware as described in detail above, in order to eliminate the possibility of Ge nanowire growth occurring from iron, chromium or nickel in the stainless steel cell walls. These experiments proved to be successful as Ge nanowires were produced with a similar yield and quality to those produced in the higher pressure experiments. An example of a nanowire synthesized at 673 K can be seen in the HRTEM micrograph in figure 6(a). The nanowire is 8 nm in diameter and exhibits a <110> crystal growth direction. Worthy of note here is that the high pressure approach is still required for synthesis at temperatures above 703 K due to thermal limitations of conventional high boiling point solvents (octacosane (b.p. 703 K) and squalane (b.p. 693 K)) thus ruling out a solution phase approach. All glassware was cleaned with aqua regia prior to use in these experiments to remove any trace metals present. Furthermore, the precursor solution was not brought into contact with any metals prior to, or during the nanowire synthesis. Every effort was also made to ensure the absence of impurities in the precursor solution which might induce nanowire growth. Previously, Chockla *et al.*[33] reported the growth of Ge nanowires via the thermal dissociation of diphenylgermane in dotriacontane. Detailed investigations of this process revealed that NaCl impurities were responsible for initiating nanowire growth. However, thermal decomposition of diphenylgermane in each of the solvents used in our study did not produce any nanowires, suggesting that the presence of a Si-based material is crucial to facilitate nanowire growth in the absence of a foreign metal catalyst.

In order to investigate the early stages of Ge nanowire growth from $Ge_2(TMS)_6$, a precursor solution was heated to 573 K for 24 h. The resulting product was composed primarily of large particles from which Ge nanowires, with a mean diameter of approximately 6 nm, protruded. Figure 6(b) shows a HRTEM micrograph of a nanowire synthesized at 573 K. The nanowire does not possess an amorphous coating and has no apparent surface oxide. No seed particles were observed at the tips of the nanowires

protruding from the microparticles suggesting that a root growth process is in operation here if a VLS-type growth mechanism is to be invoked. Figure 6(c) shows a HRTEM image of the tip of one such nanowire. The nanowire was 4.3 nm in diameter and a <211> growth direction can be elucidated from the FFT pattern (inset).

A HRTEM micrograph of Ge nanoparticles which are abundant within the silicon-based matrix at the early stages of nanowire growth is shown in figure 7. The nanoparticles are essentially Ge nuclei that did not produce nanowires, either because there was insufficient Ge feedstock remaining to fuel the particles for nanowire growth, or because the particles were isolated from the Ge feedstock by the silicon-based matrix. The nanoparticles reveal an interplanar spacing of 0.4 nm, which corresponds to {110} planes in cubic Ge. The lower magnification TEM image (inset lower left) in figure 7 shows the relative abundance of these nanoparticles at the early stages of nanowire growth. The presence of the silicon-based matrix is critical to separate these Ge nanoparticle seeds, thus preventing aggregation of nanoparticles and promoting Ge nanowire growth. It is for this reason that the structure, and the Si:Ge ratio of the $Ge_2(TMS)_6$ and $HGe(TMS)_3$ precursors is important.

A further experiment was performed in order to investigate the influence of the cooling rate on the products recovered when shorter synthesis times were used. This involved heating the precursor solution to 673 K for 24 h, at which point the solution was quenched in a flask of liquid nitrogen. The product observed was similar to that observed in figure 7, and an example of this product can be found in figure S8 in supporting information.

The growth of Ge nanowires from $Ge_2(TMS)_6$ and $HGe(TMS)_3$ can be divided into a number of stages. Firstly, the precursor must decompose to liberate Ge atoms. The strengths of the bonds present in this compound reveal that the Ge-Ge bond is the weakest (D_0(298 K) = 263.6 kJ mol^{-1}) followed by the Ge-Si bond (D_0(298 K) = 296.4 kJ mol^{-1}). The bond dissociation energy for a Si-C bond is significantly

higher (D_0(298 K) = 451.5 kJ mol^{-1}).[28] Therefore Ge atoms will be liberated first prior to the decomposition of the trimethylsilyl groups. The Ge atoms then begin to nucleate and exist as liquid droplets at a synthesis temperature of 673 K until they reach a critical diameter of ~7 nm, at which point they begin to solidify.[9, 34] Silicon-based material derived from the trimethylsilyl groups of the precursor, forms a matrix and essentially acts to separate the Ge nuclei preventing them from aggregating and forming solid particles. This matrix thus allows molten Ge droplets to exist, as it prevents the Ge particles from sintering. It is unclear why Ge nanowires would spontaneously form from Ge droplets via a VLS-type mechanism given the cubic symmetry of the Ge crystal lattice. As such, a conventional VLS mechanism may not be applicable here, and unidirectional crystal growth may involve another less conventional growth mechanism which shall be discussed later.

Coagulation of nuclei to diameters greater than 7 nm could result in two possible outcomes. Firstly, these nuclei could continue aggregating and form larger particles which have been observed in samples of the nanowire material produced here. Another possibility is that these larger nuclei which are expected to exist in a solid state at the synthesis temperature could produce nanowires via a solid phase seeding mechanism. Ge nanowires seeded from solid particles have been shown to exhibit slower growth kinetics than those seeded from liquid seed droplets.[35] Larger diameter nanowires may therefore be expected to be shorter in length due to their slower growth kinetics. However, studies have also shown that the nanowire growth rate to be proportional to diameter, giving larger diameter nanowires faster growth kinetics in CVD-based experiments.[36] The result is that no significant variation in the length of nanowires was observed for the range of diameters produced here.

Following nanowire growth, a non-uniform amorphous shell of the matrix material was found to deposit around the nanowires. This shell material is composed of Si, Ge, C and O and can be thought of as decomposed precursor material that did not produce nanowires. The shell acts to passivate the crystalline Ge nanowire surface rendering the nanowires resistant to atmospheric oxidation. For

example, the nanowire displayed in figure 3(c) was stored in air for 6 months prior to TEM analysis, and as shown by the FFT pattern (figure 3(b)), its crystallinity remains. The amorphous shell may also improve the electrical transport properties of the nanowires by saturating any dangling bonds at the surface of the Ge crystal, thus potentially removing surface states which can act to trap charge carriers in the crystal. The Si-based shell would also prevent the formation of a Ge/GeO_x interface which is undesirable due to the instability of GeO_x.[37] Notably, nanowires produced at higher temperatures invariably possessed thicker amorphous shells than those produced at lower temperatures. In fact, many nanowires produced at 573 K (figure 6(b)) did not exhibit any visible amorphous shell ,suggesting that the amorphous shell forms in a separate step after growth of the nanowire core.

As stated earlier, a VLS growth mechanism is not a likely explanation for the production of Ge nanowires from Ge nanoparticles observed in the present work. However, a number of other nanowire growth mechanisms should also be considered. A similar formation mechanism as described for oxide-assisted growth (OAG) could be possible, as the amorphous shell material here could also be considered as an inert backbone facilitating nanowire growth. Reports on the OAG mechanism state that a monoxide species such as SiO is a prerequisite for nanowire growth. This oxide acts as a sink for the vapor phase feedstock needed for nanowire growth, whilst also capping lateral growth of the nanowire. To date, there have been no reports of solution phase or supercritical fluid phase OAG of semiconductor nanowires, nor has there been any report of diameter control in nanowires produced by the OAG method. However, OAG of Ge nanowires requires the presence of a Ge species and an oxide species in equal measures to facilitate nanowire growth. As such, an OAG mechanism cannot explain the nanowire growth observed here, given the great care taken to eliminate water and oxygen from the synthesis process.

Soft templating is another potential route to nanowire production in the absence of catalytic growth seeds. This approach involves ligand control strategies for nanowire synthesis. Essentially, a ligand or

surfactant is used to cap crystal growth in certain directions, thus facilitating unidirectional nanowire growth.[38, 39] An inherent structural anisotropy is generally required to allow unidirectional growth of crystals by this method. However, reports do exist for cubic metals such as Au.[40] Consequently, it is possible that the Si-based matrix present in this work plays the role of a soft template, thus guiding nanowire growth.

Nucleation of nanowires by oriented attachment has also been reported for a number of compound semiconductors such as CdS,[41] CdTe,[42] and PbS.[43] The oriented attachment of nanoparticles of these compounds to form unidirectional structures has been attributed to the formation of a permanent or temporary electric (or magnetic) dipole in each nanocrystal. This mechanism is plausible for ionic structures consisting of layers of cations and anions, but unlikely for cubic Ge. However, oriented attachment has also been observed for metals such as Au where long-lived dipoles are unexpected.[44, 45] A complete understanding of oriented attachment in the case of highly symmetric cubic materials such as Au has not yet been achieved. Halder *et. al.*[44] suggested that a smoothing process at the interface between two fusing particles would provide sufficient asymmetry in the structure to produce a temporary electric dipole which would then act as the driving force for further particle attachment forming an elongated nanowire structure. Such a smoothing effect could be explained by the negative chemical potential expected at the interface between the particles due to the concave curvature at this interface. This negative chemical potential would provide a thermodynamic driving force for the smoothing effect and facilitate an oriented attachment growth mechanism for nanowires of cubic crystalline materials. If the observed correlation between nanowire diameter and the depressed melting point of Ge at the nanoscale is coupled to the possibility of an oriented attachment growth mechanism for Ge nanowires, a plausible growth mechanism for the nanowires produced in this study can be formulated.

As stated earlier, the Ge nanoparticles observed at the early stages of Ge nanowire growth, as shown in figure 7, are expected to exist in a semi-molten state as they are near to their theoretical melting point. These particles should readily fuse with one another, solidifying as they do so. Smoothing of the elongated structure formed, would then allow further particle attachment in accordance with previous reports on the oriented attachment of nanoparticles. Furthermore, the high curvature at the ends of these elongated structures would suggest that their tips would exist in a semi-molten state during nanowire growth. These semi-molten regions would encourage further particle attachment and one-dimensional growth. The nanowire shown in figure 6(b) displays a hallmark of this mechanism to the right of the image where two thicker sections of nanowire are separated by a thinner section suggesting that two particles may have fused at this point. Ge nanoparticles are rarely seen when nanowire growth is complete. This suggests that the nanoparticles are involved in the nanowire growth process and oriented attachment is a viable route to nanowire formation. The authors suggest that this process of semi-molten particle fusion, is the likely nanowire growth mechanism at play in the present work.

Conclusions

In conclusion, this work has demonstrated that highly crystalline Ge nanowires exhibiting diameters as small as 4 nm can be synthesized in the absence of a conventional foreign metal catalyst such as colloidal gold nanoparticles. Conventionally, foreign seed crystals and porous templates have been the only routes that allow diameter control of Ge nanowires. This report suggests that the significant melting point depression of Ge and other semiconductors at the nanoscale may provide a means to predict and control the diameters of semiconductor nanowires, by careful control of synthesis temperature, and precursor design.

Acknowledgements

We acknowledge financial support from the Irish Research Council for Science, Engineering and Technology (IRCSET) and Science Foundation Ireland (Grant 07/RFP/MASF710). This research was also enabled by the Higher Education Authority Program for Research in Third Level Institutions (2007-2011) via the INSPIRE programme.

Supporting Information Available

FTIR spectra, and additional TEM micrographs are supplied in the supporting information. This material is available free of charge via the Internet at http://pubs.acs.org.

Figures

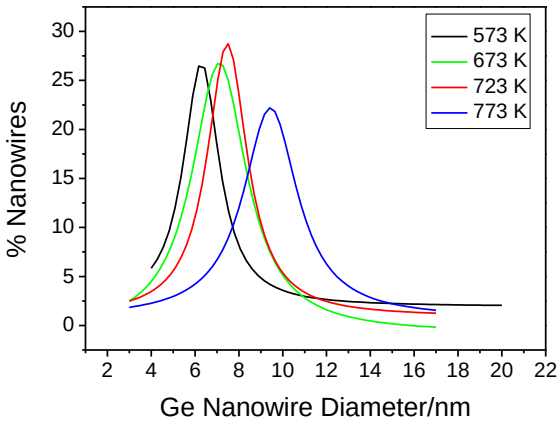

Figure 1. Lorentzian Ge nanowire diameter distributions obtained at four different synthesis temperatures. The centers of the distributions are 6.3 nm, 7.1 nm, 7.5 nm, and 9.4 nm for temperatures of 573 K, 673 K, 723 K and 773 K respectively.

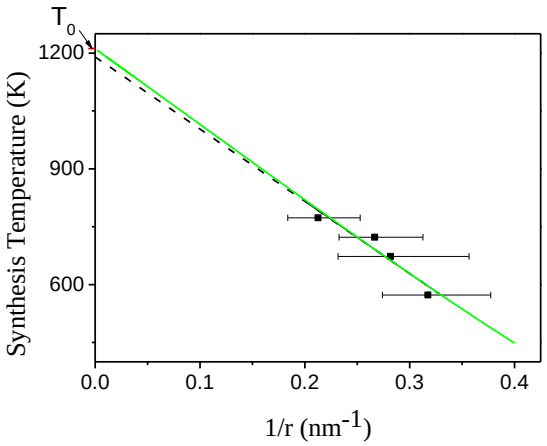

Figure 2. Plot of synthesis temperature against the inverse of the corresponding nanowire radius. The four data points from this work are highlighted. Error bars represent the full width at half maximum (FWHM) of the Lorentzian fits in figure 1. The dashed line represents a linear regression of these four points, extrapolated to intercept the y-axis. The green trace represents the theoretical melting point at the nanoparticle-nanowire interface in a VLS grown Ge nanowire by the Lindemann model. The bulk melting point of Ge (1211 K) is clearly marked on the y-axis.

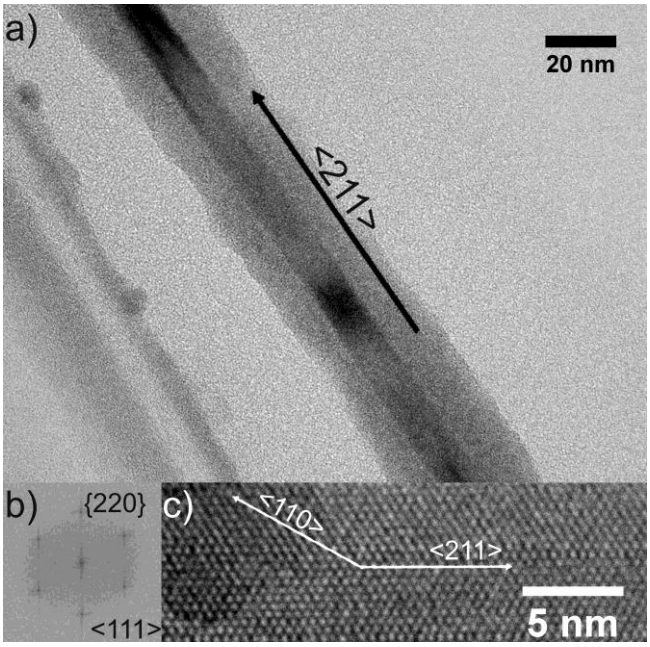

Figure 3. (a) TEM micrograph of a typical nanocable synthesized at 773 K, showing the distinct core-shell morphology. (b) Inset, a fast Fourier transform (FFT) of the HRTEM image in (c), highlighting a low defect density in the crystalline Ge nanowires, (c) HRTEM micrograph of a similar 10 nm diameter Ge nanowire to that shown in (a). The image was obtained along the <111> zone axis of the Ge nanowire.

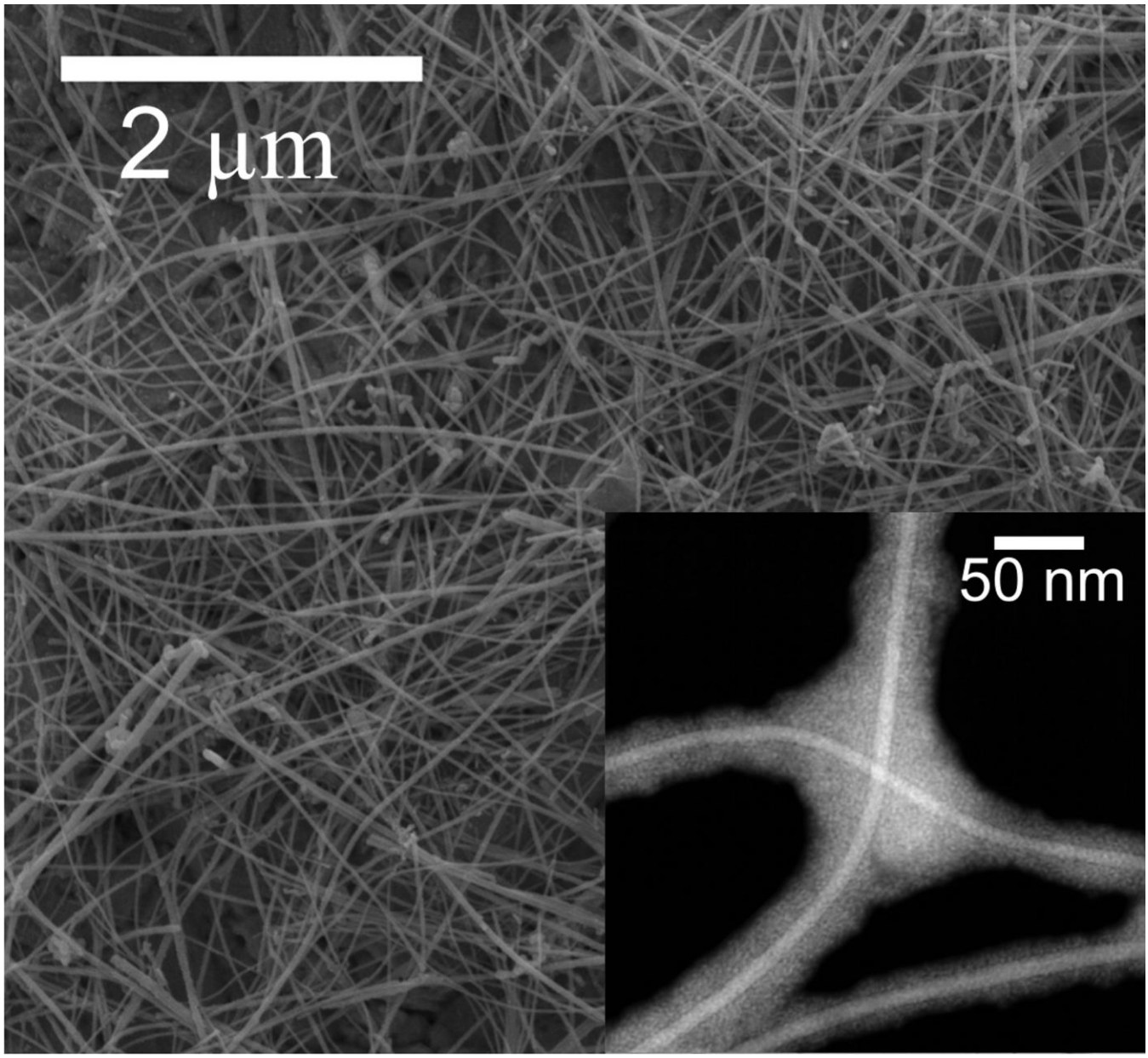

Figure 4. A SEM micrograph of the Ge nanowires produced in this work. Inset is a HAADF STEM micrograph of Ge nanowires synthesised at 673 K, clearly displaying the core-shell morphology of several Ge nanowires. Including shell, the nanowires shown are 20 to 50 nm in diameter, whilst the cores are 8 to 10 nm in diameter and show good uniformity along the wires.

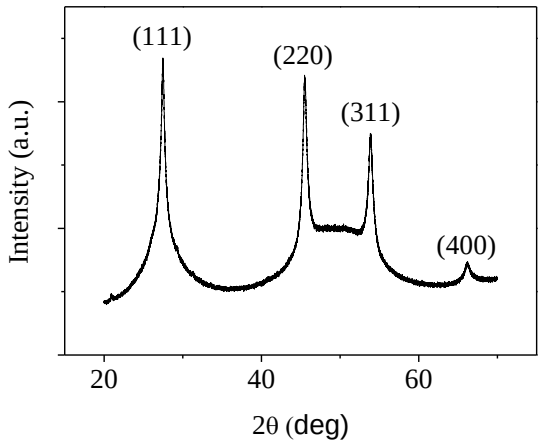

Figure 5. PXRD pattern of a sample of Ge nanowires synthesized at 673 K. All reflections can be indexed to cubic Ge (JCPDS, reference pattern 04-0545, space group *Fd3m*). The broad hump in the background observed between the (220) and (311) reflections is due to amorphous Si-based material present in the sample.

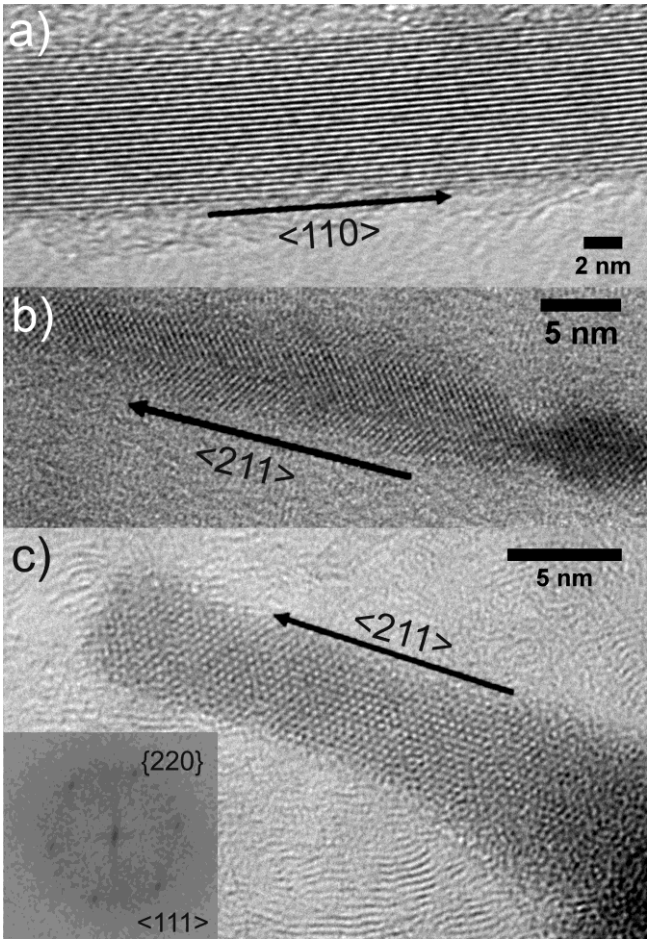

Figure 6. (a) HRTEM micrograph of an 8 nm diameter Ge nanowire synthesized at 673 K, (b) HRTEM micrograph of a Ge nanowire observed during the early stages of growth. The wire has a <211> growth direction and the {110} atomic planes are visible at 60° to the growth axis. No surface oxide layer was observed on the nanowire surface. (c) The tip of a Ge nanowire protruding from a largely amorphous microparticle. Inset, a FFT of the nanowire, which confirms that it is single crystalline in the region shown, and has a <211> growth direction.

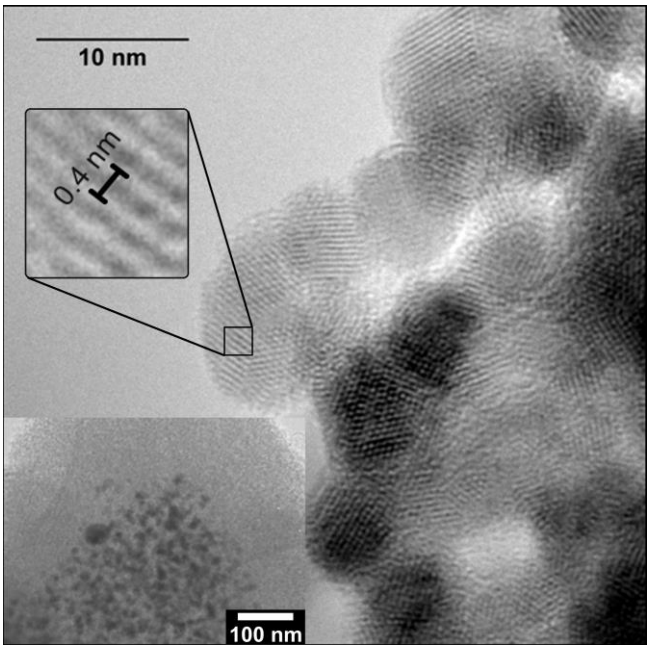

Figure 7. HRTEM micrograph of aggregated Ge nanoparticles observed at the surface of Si rich microparticles. Inset bottom left, a lower magnification TEM image of similar nanoparticles showing the surrounding Si based matrix, scale bar 100 nm.

References

(1) Barth, S.; Hernandez-Ramirez, F.; Holmes, J. D.; Romano-Rodriguez, A. *Prog. Mater. Sci.* **2010**, *55*, 563.
(2) International Technology Roadmap for Semiconductors, 2007 Executive Summary http://www.itrs.net/.
(3) Sze, S. M. *Semiconductor Devices: Physics and Technology*, 1st ed.; Wiley: New York, 1985.
(4) Liang, G.; Xiang, J.; Kharche, N.; Klimeck, G.; Lieber, C. M.; Lundstrom, M. *Nano Lett.* **2007**, *7*, 642.
(5) Wagner, R. S.; Ellis, W. C. *Appl. Phys. Lett.* **1964**, *4*, 89.
(6) Gu, G.; Burghard, M.; Kim, G. T.; Düsberg, G. S.; Chiu, P. W.; Krstic, V.; Roth, S.; Han, W. Q. *J. Appl. Phys.* **2001**, *90*, 5747.
(7) Perea, D. E.; Hemesath, E. R.; Schwalbach, E. J.; Lensch-Falk, J. L.; Voorhees, P. W.; Lauhon, L. J. *Nat. Nano.* **2009**, *4*, 315.
(8) Schmidt, V.; Wittemann, J. V.; Senz, S.; Gösele, U. *Adv. Mater.* **2009**, *21*, 2681.
(9) Ge, M.; Liu, J. F.; Wu, H.; Yao, C.; Zeng, Y.; Fu, Z. D.; Zhang, S. L.; Jiang, J. Z. *J. Phys. Chem. C* **2007**, *111*, 11157.
(10) Patterson, A. L. *Phys. Rev.* **1939**, *56*, 978.
(11) Zaitseva, N.; Harper, J.; Gerion, D.; Saw, C. *Appl. Phys. Lett.* **2005**, *86*, 053105.
(12) Zhang, Y. F.; Tang, Y. H.; Wang, N.; Lee, C. S.; Bello, I.; Lee, S. T. *Phys. Rev. B* **2000**, *61*, 4518.
(13) Meng, X. M.; Hu, J. Q.; Jiang, Y.; Lee, C. S.; Lee, S. T. *Appl. Phys. Lett.* **2003**, *83*, 2241.
(14) Mathur, S.; Shen, H.; Donia, N.; Rugamer, T.; Sivakov, V.; Werner, U. *J. Am. Chem. Soc.* **2007**, *129*, 9746.
(15) Gerung, H.; Boyle, T. J.; Tribby, L. J.; Bunge, S. D.; Brinker, C. J.; Han, S. M. *J. Am. Chem. Soc.* **2006**, *128*, 5244.
(16) Cui, Y.; Lauhon, L. J.; Gudiksen, M. S.; Wang, J.; Lieber, C. M. *Appl. Phys. Lett.* **2001**, *78*, 2214.
(17) Holmes, J. D.; Johnston, K. P.; Doty, R. C.; Korgel, B. A. *Science* **2000**, *287*, 1471.
(18) Lombardi, I.; Hochbaum, A. I.; Yang, P.; Carraro, C.; Maboudian, R. *Chem. Mater.* **2006**, *18*, 988.
(19) Adhikari, H.; Marshall, A. F.; Goldthorpe, I. A.; Chidsey, C. E. D.; McIntyre, P. C. *ACS Nano* **2007**, *1*, 415.
(20) Woodruff, J. H.; Ratchford, J. B.; Goldthorpe, I. A.; McIntyre, P. C.; Chidsey *Nano Lett.* **2007**, *7*, 1637.
(21) Arnold, D. C.; Hobbs, R. G.; Zirngast, M.; Marschner, C.; Hill, J. J.; Ziegler, K. J.; Morris, M. A.; Holmes, J. D. *J. Mater. Chem.* **2009**, *19*, 954.
(22) Fischer, J.; Baumgartner, J.; Marschner, C. *Organometallics* **2005**, *24*, 1263.
(23) Hanrath, T.; Korgel, B. A. *J. Am. Chem. Soc.* **2002**, *124*, 1424.
(24) Heitsch, A. T.; Fanfair, D. D.; Tuan, H.-Y.; Korgel, B. A. *J. Am. Chem. Soc.* **2008**, *130*, 5436.
(25) Lindemann, F. R. *Z. Phys.* **1910**, *11*, 609.
(26) Dash, J. G. *Rev. Mod. Phys.* **1999**, *71*, 1737.
(27) Zhang, Z.; Zhao, M.; Jiang, Q. *Semicond. Sci. Technol.* **2001**, *16*, L33.
(28) "Molecular Structure and Spectroscopy", in *CRC Handbook of Chemistry and Physics*, *Internet Version 2005,* D.R. Lide, ed, http://www.hbcpnetbase.com, CRC Press, Boca Raton, FL, 2005.
(29) Wacaser, B. A.; Dick, K. A.; Johansson, J.; Borgström, M. T.; Deppert, K.; Samuelson, L. *Adv. Mater.* **2009**, *21*, 153.
(30) Schmidt, V.; Senz, S.; GÃ¶sele, U. *Nano Lett.* **2005**, *5*, 931.
(31) Choi, W. K.; Natarajan, A.; Bera, L. K.; Wee, A. T. S.; Liu, Y. J. *J. Appl. Phys.* **2002**, *91*, 2443.
(32) Rodriguez, A.; Ortiz, M. I.; Sangrador, J.; Rodriguez, T.; Avella, M.; Prieto, A. C.; Torres, A.; Jimenez, J.; Kling, A.; Ballesteros, C. *Nanotechnology* **2007**, *18*, 065702.

(33) Chockla, A. M.; Korgel, B. A. *J. Mater. Chem.* **2009**, *19*, 996.
(34) Wu, Y.; Yang, P. *Adv. Mater.* **2001**, *13*, 520.
(35) Kodambaka, S.; Tersoff, J.; Reuter, M. C.; Ross, F. M. *Science* **2007**, *316*, 729.
(36) Kashchiev, D. *Cryst. Growth Des.* **2006**, *6*, 1154.
(37) Wang, D.; Chang, Y.-L.; Wang, Q.; Cao, J.; Farmer, D. B.; Gordon, R. G.; Dai, H. *J. Am. Chem. Soc.* **2004**, *126*, 11602.
(38) Cademartiri, L.; Ozin, G. A. *Adv. Mater.* **2009**, *21*, 1850.
(39) Tao, A. R.; Habas, S.; Yang, P. *Small* **2008**, *4*, 310.
(40) Jana, N. R.; Gearheart, L.; Murphy, C. J. *J. Phys. Chem. B* **2001**, *105*, 4065.
(41) Ryan, K. M.; Mastroianni, A.; Stancil, K. A.; Liu, H.; Alivisatos, A. P. *Nano Lett.* **2006**, *6*, 1479.
(42) Tang, Z.; Kotov, N. A.; Giersig, M. *Science* **2002**, *297*, 237.
(43) Patla, I.; Acharya, S.; Zeiri, L.; Israelachvili, J.; Efrima, S.; Golan, Y. *Nano Lett.* **2007**, *7*, 1459.
(44) Wang, C.; Hu, Y.; Lieber, C. M.; Sun, S. *J. Am. Chem. Soc.* **2008**, *130*, 8902.
(45) Halder, A.; Ravishankar, N. *Adv. Mater.* **2007**, *19*, 1854.

Table of Contents Figure